Ecological Applications, 29(2), 2019, e01834
Published 2018. This article is a U.S. Government work and is in the public domain in the USA

Assessing regional drought impacts on vegetation and evapotranspiration: a case study in Guanacaste, Costa Rica

Savannah S. Cooley,[1,2,4] Christopher A. Williams,[2] Joshua B. Fisher,[1] Gregory H. Halverson,[1] Johan Perret,[3] and Christine M. Lee[1]

[1] *Jet Propulsion Laboratory, California Institute of Technology, Pasadena, California 91109 USA*
[2] *Clark University Graduate School of Geography, Worcester, Massachusetts 01610 USA*
[3] *EARTH University, Limón Province, Mercedes, Costa Rica*

Citation: Cooley, S. S., C. A. Williams, J. B. Fisher, G. H. Halverson, J. Perret, and C. M. Lee. 2019. Assessing regional drought impacts on vegetation and evapotranspiration: a case study in Guanacaste, Costa Rica. Ecological Applications 29(2):e01834. 10.1002/eap.1834

Abstract. This research investigates ecological responses to drought by developing a conceptual framework of vegetation response and investigating how multiple measures of drought can improve regional drought monitoring. We apply this approach to a case study of a recent drought in Guanacaste, Costa Rica. First, we assess drought severity with the Standard Precipitation Index (SPI) based on a 64-yr precipitation record derived from a combination of Global Precipitation Climatology Center data and satellite observations from Tropical Rainfall Measuring Mission and Global Precipitation Measurement. Then, we examine spatial patterns of precipitation, vegetation greenness, evapotranspiration (ET), potential evapotranspiration (PET), and evaporative stress index (ESI) during the drought years of 2013, 2014, and 2015 relative to a baseline period (2002–2012). We compute wet season (May–October) anomalies for precipitation at 0.25° spatial resolution, normalized difference vegetation index (NDVI) at 30-m spatial resolution, and ET, PET and ESI derived with the Priestley-Taylor Jet Propulsion Laboratory (PT-JPL) model at 1-km spatial resolution. We assess patterns of landscape response across years and land cover types including three kinds of forest (deciduous, old growth, and secondary), grassland, and cropland. Results show that rainfall in Guanacaste reached an all-time low in 2015 over a 64-yr record (wet season SPI = −3.46), resulting in NDVI declines. However, ET and ESI did not show significant anomalies relative to a baseline, drought-free period. Forests in the region exhibited lower water stress compared to grasslands and had smaller declines, and even some increases, in NDVI and ET during the drought period. This work highlights the value of using multiple measures to assess ecosystem responses to drought. It also suggests that agricultural land management has an opportunity to integrate these findings by emulating some of the characteristics of drought-resilient ecosystems in managed systems.

Key words: agricultural land management; Costa Rica; drought response; ecosystem sensitivity; evapotranspiration; Guanacaste; remote sensing; vegetation index.

Introduction

Background and motivation

Precipitation deficits are usually the first measure of drought and often have immediate impacts on the landscape, causing increased vegetation stress. In particular, arid biomes tend to respond to drought at short time scales, likely due to the plant species of arid regions having evolved to rapidly adapt to changing water availability (Vicente-Serrano et al. 2013). Humid biomes also respond to drought at short time scales, but in this case the physiological mechanisms likely differ from those in arid biomes, as plants usually have a poor adaptability to water shortage. It is common to use precipitation-based drought measures alone, with an assumption, often implicit, that observed decreases in rainfall have proportional increases in vegetation stress during the same time period as the drought (Sönmez et al. 2005, Patel et al. 2007).

This study develops a conceptual framework of drought characterization depicting multiple possible vegetation responses to precipitation deficits so that differences among drought response in vegetation are explicit (Fig. 1). Within the conceptual framework, Scenario A shows a situation in which vegetation is highly sensitive to drought and exhibits stress immediately following the decrease in precipitation. However, precipitation deficits do not necessarily cause immediate increases in vegetation stress. Therefore, in Scenario B, the landscape experiences a lag after a precipitation deficit before vegetation stress increases. Vicente-Serrano et al. (2013), for instance, found that semiarid and subhumid biomes

Manuscript received 22 March 2018; revised 11 September 2018; accepted 10 October 2018. Corresponding Editor: Nancy F. Glenn.
[4] E-mail: savannah.s.cooley@jpl.nasa.gov

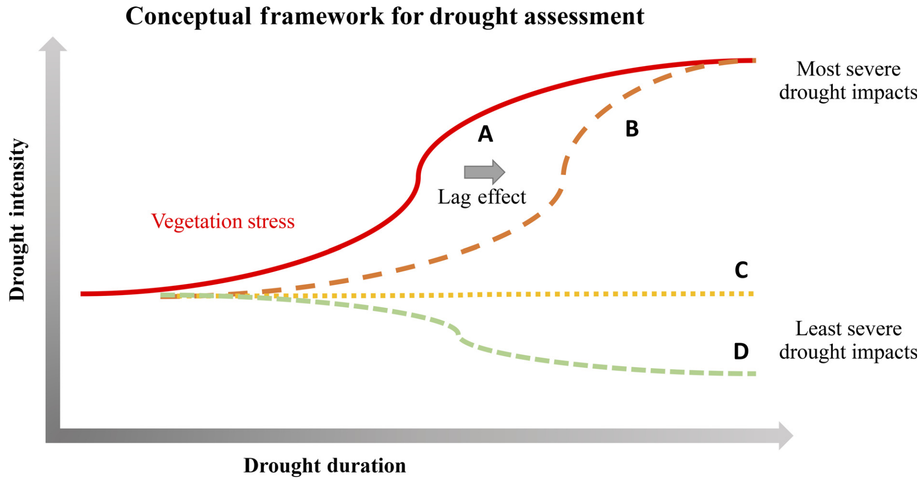

FIG. 1. The conceptual framework for drought assessment depicts drought duration on the *x*-axis and drought impacts in terms of vegetative stress on the *y*-axis. Vegetation stress can be measured both in terms of normalized difference vegetation index (NDVI) and evaporative stress index (ESI; evapotranspiration [ET]/potential evapotranspiration [PET]). The framework assumes a constant precipitation deficit across the time period covered. Scenario A captures a drought response where vegetation stress increases immediately as a result of the precipitation deficit. However, other possible drought responses in vegetation include (B) experiencing a lag to a precipitation deficit before increasing stress, (C) not experiencing any changes in stress, or (D) decreasing vegetation stress.

respond to drought at long time scales, probably because plants are able to withstand water deficits, but they lack the rapid response of arid biomes to drought. In Scenario C, no changes in vegetation stress can be attributed to the drought, which often arises when the intensity or duration of drought are low relative to other droughts in the region. The magnitude of drought that characterized the 1930s in Nebraska, for example, was enough to disturb fine-grained farm soils and the crops growing on them, but did not impact naturally vegetated areas (Muhs 1998, Mangan et al. 2004). In some cases, at least in the short term, vegetation greening can occur, indicating a decrease in vegetation stress. Scenario D represents this case. For example, Saleska et al. (2007) showed a large-scale photosynthetic green-up in intact evergreen forests of the Amazon in response to a short, intense drought in 2005.

The reliability and usefulness of meteorological drought indices solely based on precipitation measurements are limited by spatial distribution, quality of data and ability to reflect only one component of the surface hydrologic cycle (Anderson et al. 2011). Precipitation-based assessments of drought frequently miss an opportunity to evaluate the impact rainfall deficits have on the landscape, which varies spatially and temporally, depending on water availability, atmospheric demand, and vegetation resilience (Penuelas et al. 2004). Evapotranspiration (ET) data can complement precipitation-based drought assessment. They capture non-precipitation-based moisture inputs to the land surface system, such as irrigation, that may alter drought impacts or rates of water consumption across a landscape (Senay et al. 2007, Otkin et al. 2013). Empirical indices measuring anomalies in vegetation condition (e.g., the normalized difference vegetation index, NDVI) are useful for monitoring drought response over large areas (Peters et al. 2002) but may provide ambiguous results when other factors such as air temperature and advection affect plant functioning (Kustas et al. 2011). Precipitation and vegetation-based drought indicators also miss the role of evaporative demand in driving plant stress and drought impacts, which potential ET (PET) captures (Tsakiris et al. 2007, Vicente-Serrano et al. 2013).

Anderson et al. (2011) assess the impacts of drought utilizing the evaporative stress index (ESI), which quantifies the ratio of ET to PET. Normalization by PET serves to isolate the ET signal component responding to soil moisture variability from variations due to the radiation load. Spatial and temporal correlation analyses suggest that the ESI performs similarly to short-term (up to 6 months) precipitation-based indices but can be produced at finer spatial resolution and without requiring any precipitation data.

This research uses a case study in Guanacaste, Costa Rica, to assess drought severity in the context of the conceptual drought assessment framework by measuring regional patterns in precipitation and characterizing drought impact on vegetation stress with NDVI and ESI (ET/PET). We derived the ET and PET products using the Priestley-Taylor Jet Propulsion Laboratory (PT-JPL) model (Fisher et al. 2008) in order to effectively capture both agricultural and non-agricultural landscapes. Mapping evapotranspiration at high resolution with internalized calibration (METRIC) developed by Allen et al. (2005) and the Atmosphere-Land Exchange Inverse (ALEXI) model developed by Anderson et al. (2007) were designed to measure ET for primarily agriculture applications. The PT-JPL model, on the other hand, was developed for a wide range of natural ecosystems.

PT-JPL translates Priestley-Taylor estimates of PET (Priestley and Taylor, 1972) into rates of ET through applying biophysical constraints to PET. Rather than relying on soil moisture, stomatal resistance and wind speed data, which are unavailable in most parts of the world (De Bruin and Stricker 2000), PT-JPL assesses plant physiological limitations of transpiration, interception, and soil evaporation constraints using NDVI, soil adjusted vegetation index (SAVI), relative humidity, and fractional vegetation cover estimates.

Study aims and hypotheses

The aim of this study was to investigate how multiple measures of vegetation response, including remote sensing-based vegetation indices and evapotranspiration data, vary across time and space, with a particular focus on the way the variables complement one another to provide a holistic approach to drought assessment. One of the hypotheses explored in this study is that drought impacts on the landscape do not always arise immediately after a precipitation deficit (Scenario A of the conceptual framework for drought assessment); rather, they tend to often have lagged impacts (Scenario B), no detectable impacts (Scenario C), or even increases in vegetation stress (Scenario D).

Anomalies in NDVI can indicate changes of plant health over time by detecting the change in the amount of photosynthetic vegetation present in a landscape (Pettorelli et al. 2005). Meanwhile, ET anomalies represent changes in a biophysical plant process of carbon and water exchange, which relates to atmospheric demand, soil moisture conditions and plant stress (Fisher et al. 2011). ESI provides a measure of ET that explicitly normalizes for PET. For this reason, while ET, ESI, and NDVI each provide different information related to vegetation health, we expect them to yield similar results in the drought detection analysis of Guanacaste. This is so because when vegetation is stressed by a lack of water, the results appear in both the photosynthetic vegetation (as measured by NDVI) and the capacity of ET that vegetation is able to maintain given a specific PET quantity (as measured by ESI; Karnieli et al. 2010, DeJong et al. 2012). However, the timing of these responses can often be decoupled, with changes in ET and ESI often being earlier drought warning signs compared to NDVI (Anderson et al. 2011).

Another hypothesis that builds on the conceptual framework for drought assessment is that the drought-propagated vegetation stress (as measured by NDVI, ET, and ESI) varies significantly within the landscape. This suggests that certain habitat types are more drought resilient than others, as local edaphic properties affect tropical forest structure and function (Quesada and Lloyd 2016). Hofhansl et al. (2014) reached a similar conclusion by analyzing climate sensitivity of tropical forest aboveground net primary production in Costa Rica. They conclude that the impact of climate anomalies on tropical forest productivity is strongly related to local site characteristics including local topography and disturbance history. Local conditions will therefore likely prevent uniform responses of tropical lowland forests to projected global changes.

We expect to see an oscillating pattern of positive correlation to negative correlation between the raw precipitation time series and the measures of vegetation stress (NDVI, ET, and ESI). Specifically, we hypothesize that at the beginning of the wet season, the drought response indicators of NDVI, ET, and ESI will have a negative correlation with precipitation. Then, up to a couple months after the wet season, we expect a positive correlation with precipitation. In the dry season, we expect the same pattern but in reverse. We expect this because, in the spring and early summer for instance, precipitation begins increasing but the vegetation may not yet have had time to respond to the increase in water availability. Thus, vegetation stress remains high for a couple months, particularly for NDVI, which has shown to be a slower-moving response than ET and ESI (Anderson et al. 2011). After a few months of rainfall, vegetation stress will likely decrease.

We also hypothesize that the precipitation anomalies (monthly climatologies) will have lagging impacts on NDVI, ET, and ESI anomalies. Given the magnitude of the precipitation anomalies in the recent drought years of 2013, 2014, and 2015 along with the sub-humid climate of Guanacaste, we expect increases in vegetation stress, with a lag of up to 1 yr after the end of the drought (Vicente-Serrano et al. 2013). If the negative lags have significant correlations between precipitation anomalies and NDVI, ET, and ESI anomalies, then Scenario B provides the best fit to characterize the drought response observed in Guanacaste. If, on the other hand, the lags do not have significant correlations between precipitation anomalies and NDVI, ET, and ESI anomalies, then Scenario C or D provide the best drought characterization of Guanacaste.

The wet season in Guanacaste takes place during the summer, which has the highest amount of incoming solar radiation. Despite the increase in cloud cover associated with precipitation (which blocks some solar radiation), we hypothesize that PET and precipitation will have a positive relationship for lags close to 0 (± 2) because we expect the net radiation in the wet summer months to still be larger than the net radiation in the dry winter months. We hypothesize that PET will also have a cyclical positive to negative correlation pattern as described for the cross-correlations of NDVI, ET, and ESI.

Methods

Study area

Guanacaste is a province in northwestern Costa Rica bordering the Pacific and covers an area of 10,141 km^2. Guanacaste has a tropical savanna climate within the

Table 1. Mean temperatures and precipitation in Guanacaste Province, Costa Rica.

Parameter	Jan	Feb	Mar	Apr	May	Jun	Jul	Aug	Sep	Oct	Nov	Dec	Annual mean
Max. temp (°C)	33	35	35	36	34	32	32	32	31	31	31	31	33
Min. temp (°C)	21	21	22	23	26	23	23	23	22	22	22	22	24
Precip (mm)	16	10	13	37	184	257	190	225	322	290	117	30	1,691
Days with rain	2	0	0	3	15	24	17	19	28	26	12	4	13
Humidity (%)	66	64	61	63	74	84	80	82	86	87	81	72	75

Notes: The Costa Rica National Weather Services provided this data. In the "Precip" row, the values listed under each month are a climatology and correspond to the average of the sum of that month's total rainfall between 1951 and 2015. In the "Annual mean" column of this row, the value listed is the accumulated rainfall averaged over the same time period used to derive monthly averages (1951–2015). All values are means. Precip, precipitation; temp, temperature; max, maximum; min, minimum.

Köppen-Geiger climate classification system. The province experiences pronounced wet and dry seasonality, with almost all of the 1,691 mm of annual precipitation falling during the wet season, which spans from late May to November (Table 1). The first maximum of precipitation is followed by a dry period of two to three weeks in July, usually referred to as the midsummer drought (Magaña et al. 1999). The mean maximum temperature is 31.85°C in the wet season and 34°C in the dry season. The mean minimum temperature is 23°C in the wet season and 21.8°C in the dry season. The mountainous region in the east of Guanacaste typically experiences lower temperatures than the rest of the province due to its high elevation. The region has an average air humidity of 82.2% in the wet season and 67.8% humidity in the dry season. Guanacaste is located in the dry corridor in Central America, an area that accounts for one-third of the total land in Central America. The region is especially susceptible to the atmospheric effects of El Niño Southern Oscillation (ENSO) events (UNOCHA 2014). The 2015 ENSO conditions aggravated the onset of the most recent drought in the dry corridor, resulting in a further decrease in precipitation (UNOCHA 2016).

Forest, including deciduous forest, mature forest, and secondary forest, occupies the largest spatial extent compared to the other land cover categories of grassland and agriculture (Fig. 2). The southwestern part of the province is mostly deciduous forest, with fragments of mature forest, secondary forest, and agriculture. Mature forests are clustered in the northeast and secondary forests are clustered in the southeast. Agricultural areas are primarily in the central region of the province with smaller clusters in the northern tip and the southwest. Grassland is scattered throughout the province. Mature forests are primarily located in the northeastern area of Guanacaste. Meanwhile, the largest patch of secondary forests is in the southeastern region. Agriculture areas are primarily in the central region of the province as well as in a cluster to the north and a more dispersed group of patches in the south. Grassland is scattered throughout the province as is secondary forest. The largest patch of mature forests is in the eastern part of Guanacaste. Deciduous forest occupies the largest region in the south.

The source of the land cover data is the Sistema Nacional de Áreas de Conservación (SINAC) Unidad de Monitoreo Forestal, partially funded by the Costa Rica Fondo de Financiamiento Forestal (National Forestry Financing Fund, FONAFIFO) and the German Corporation for International Cooperation (GIZ). The data are based on the classification of Rapideye images with five spectral bands and a spatial resolution of 5 × 5 m, with an overall accuracy of the combined forest and non-forest classes ~89% (SINAC 2013). The images were taken from June 2011 to 2012. For more information about the land cover classification data, please see the SINAC documentation of the creation of the land cover data set (SINAC, 2013). We used the data produced by the basin-info network from the Tempisque-Bebedero river basin (which covers the majority of the agricultural areas of Guanacaste) to provide information on agriculture because the 2013 data from SINAC did not provide agricultural land cover information (data *available online*).[5]

Spatial anomalies of drought indicators

The overall methodology of this analysis consists of three different yet complementary approaches to characterizing the drought in Guanacaste (Fig. 3).

Standard precipitation index (SPI).—The first drought assessment approach characterizes the severity of the 2015 drought in Guanacaste using the standard precipitation index (SPI), formulated by McKee et al. (1993). SPI is the number of standard deviations by which the observed value of precipitation lies above or below the long-term mean, for a normally distributed random variable. The SPI computation with a 6-month time step represents seasonal precipitation anomalies corresponding to the wet season and the dry season. For the first part of the historic record from 1951 to 2000, this study uses precipitation data from the Global Precipitation Climatology Centre (GPCC) gridded at a 0.5° latitude/longitude resolution (for more details about the creation of the gridded monthly precipitation data and quality control, see Beck et al. 2005). For the remainder of the time period of interest from 2002 to 2015, this study uses

[5] http://www.basin-info.net/river-basins/tempisque-basin-br-costa-rica

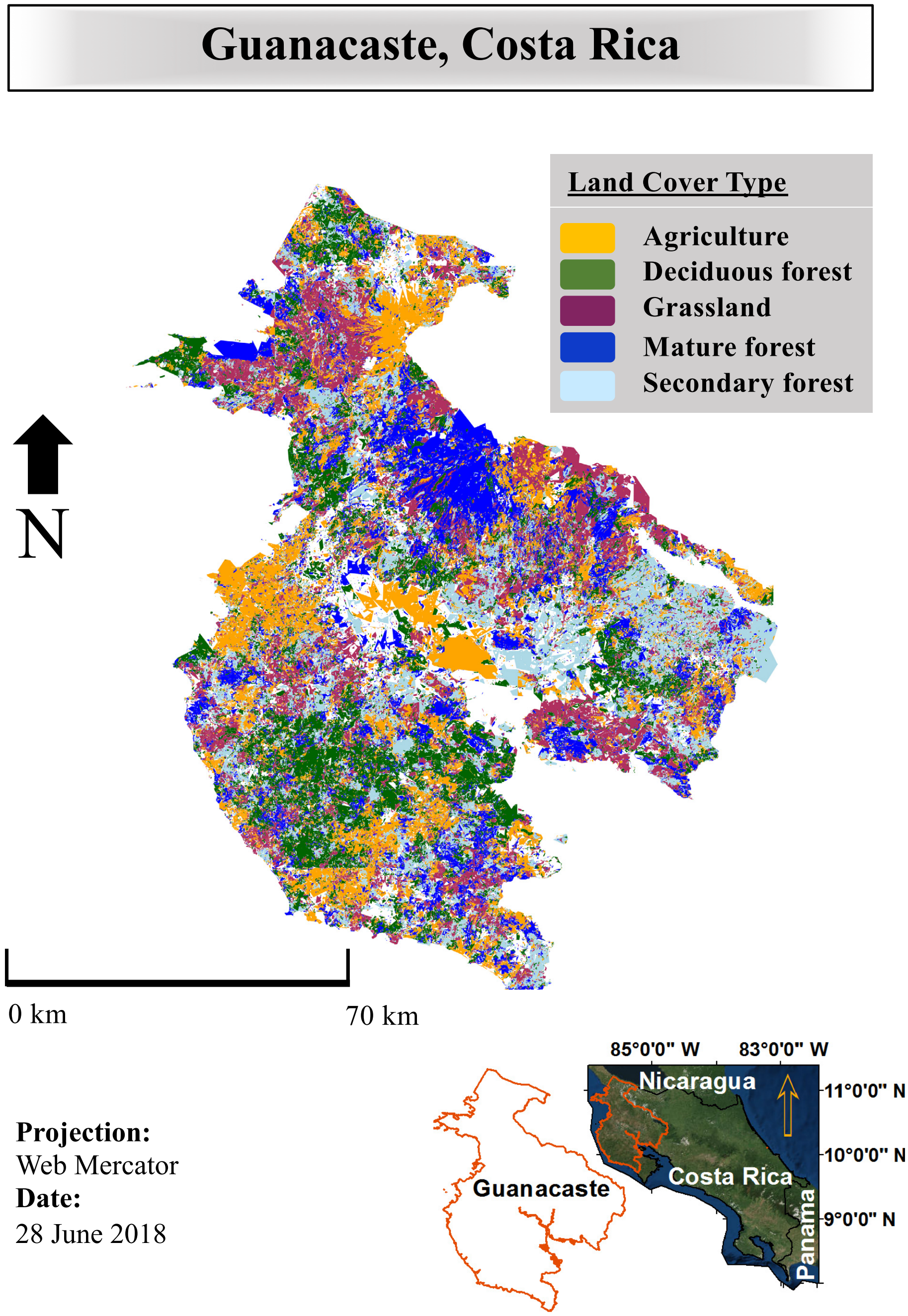

FIG. 2. Land cover map of Guanacaste. The five land cover classes include agriculture, deciduous forest, grassland, mature forest, and secondary forest. When the subcategories are aggregated together, forest covers the largest spatial extent in Guanacaste compared to agriculture and grassland. Deciduous forest is mostly in the southwest of the province. Mature forests are clustered in the northeast and secondary forests are clustered in the southeast. Agricultural areas are primarily in the central region of the province with smaller clusters in the northern tip and the southwest. Grassland is scattered throughout the province.

a monthly 0.25° resolution precipitation data set called the Multi-Satellite Precipitation Analysis Version 7 (TMPA-3B43V7), which combines the Tropical Rainfall Measuring Mission (TRMM) with the Global Precipitation Measurement (GPM) mission and other meteorological data. For both the GPCC precipitation product and the TMPA-3B43V7 product, a mean precipitation value was computed across the study area to derive mean monthly observations from 1951 through 2015 for input to the SPI computation.

Precipitation.—The low spatial resolution of the gridded GPCC precipitation data required the sole use of the 0.25° the TMPA-3B43V7 product that combines

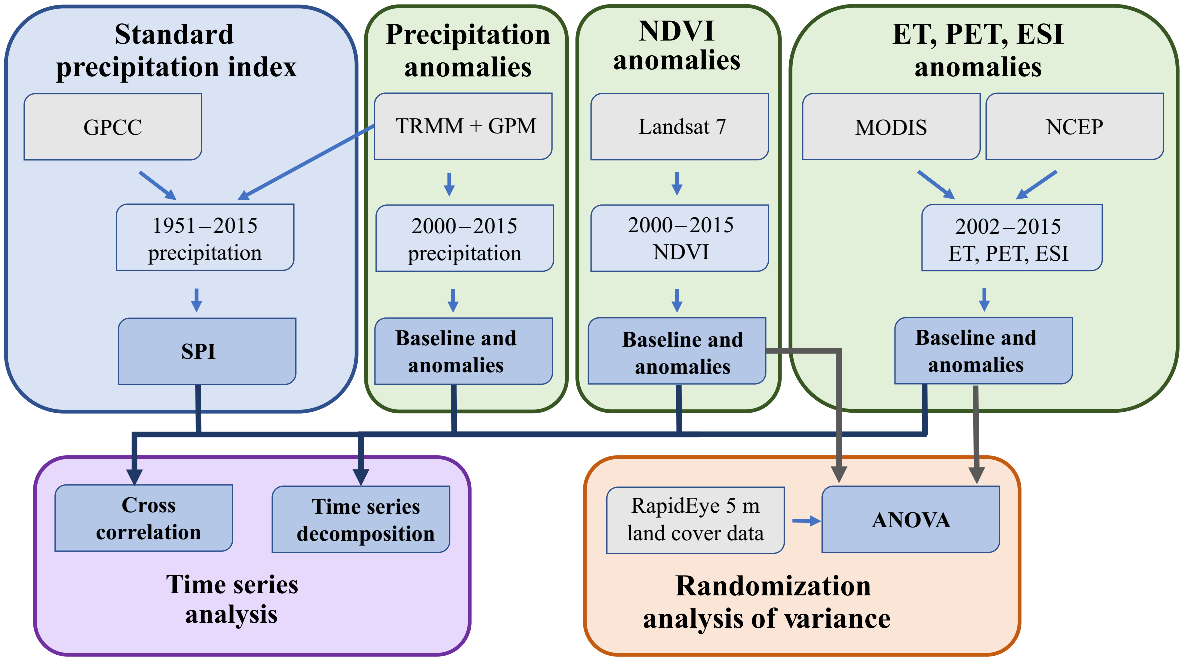

Fig. 3. Methodology used in this study. The multiple approaches to drought assessment used in the research methodology include computing standard precipitation index (SPI) as well as spatial anomalies in the drought years of 2013, 2014, and 2015 of precipitation, NDVI, ET, PET, and ESI for the wet season (May through October) in Guanacaste. The input data used to derive ET, PET, and ESI are from moderate resolution imaging spectroradiometer (MODIS) and National Centers for Environmental Prediction (NCEP) Reanalysis II. This study also computes a randomization analysis of variance (ANOVA) to test differences in drought response across land cover type, year, and season. The time series analyses include the seasonal and trend decomposition procedure (STL) and the time series cross-correlations; both of which integrate precipitation, NDVI, ET, PET, and ESI monthly means as well as monthly climatologies. GPCC, Global Precipitation Climatology Center; TRMM, Tropical Rainfall Measuring Mission; GPM, Global Precipitation Measurement Mission.

TRMM and GPM data for computing spatially explicit wet season precipitation anomalies. First, we disaggregated the data from 0.25° resolution to 1-km pixel resolution with a bilinear interpolation method and cropped the data to the boundary of Guanacaste. We converted data to monthly totals. This yielded monthly precipitation averages at 1-km spatial resolution in units of millimeters per month. We took the mean value for each pixel in the time series for May through October from 2002 to 2012 to derive the wet season baseline for precipitation. We produced season-specific anomalies by subtracting the baseline from the mean wet season values from the values during the wet seasons of each drought year (2013, 2014, and 2015).

Normalized difference vegetation index (NDVI).—We derived NDVI from Landsat 7 Surface Reflectance images spanning from 1 January 2002 to 27 December 2015, and accessed all data products from Google Earth Engine for the finer 30-m resolution vegetation drought response analysis. Google Earth Engine computed the Landsat 7 NDVI product from atmospherically corrected surface reflectance images and provided the product in a 16-d global composite with a spatial resolution of 30 m. To mask cloud cover and associated shadows, we applied a composite of the cloud mask, a band within the Landsat surface reflectance product. We computed the baseline and anomalies for NDVI with the same process as described in the previous sub-section on precipitation.

Evapotranspiration (ET), potential ET (PET), and evaporative stress index (ESI).—Computing the set of anomalies for ET, PET, and ESI involves analysis of the output from the PT-JPL model. PT-JPL uses an energy balance approach to calculate how much water loss is required to keep the soil and vegetation at the observed temperatures given known net radiation (Fisher et al. 2008). Five model inputs are required: net radiation (from the Breathing Earth System Simulator [BESS] model; see Ryu et al. 2011), NDVI, soil adjusted vegetation index (SAVI), daily maximum air temperature, and atmospheric water vapor pressure. PT-JPL is partitioned into canopy transpiration (ET_c), soil evaporation (ET_s), and interception evaporation (ET_i). Total evapotranspiration, ET, is the sum of $ET_c + ET_s + ET_i$. Canopy transpiration is the amount of water vapor lost to the atmosphere through plant tissues. Soil evaporation is the direct evaporation of water from the near surface soil. Interception evaporation is the evaporation of water that is intercepted by precipitation or fog, or deposited as dew and stored on the surface of plants. For each component flux, PT-JPL reduces PET to actual ET based on relative surface wetness, green canopy fraction, plant temperature constraint, plant moisture constraint, and soil moisture constraint. This implementation of PT-JPL calculates latent energy in W/m^2, producing an ET product with 1-km pixel cells. The primary input to PT-JPL is moderate resolution imaging spectroradiometer (MODIS) daily observations at ~10:30 from the *Terra* satellite, including the NDVI and land surface temperature data products. These data products were retrieved from two distributed active archive centers (DAACs), managed by United States Geological Survey and NASA Earth Resources Observation and Science (EROS) Center: (1) Land Processes DAAC (LP DAAC), Sioux Falls, South Dakota, USA and (2) the Level-1 and Atmosphere Archive and Distribution System (LAADS DAAC), Greenbelt, Maryland (data *available online*).[6,7] When MODIS observations were not available, the algorithm retrieves data from National Centers for Environmental Prediction to gap-fill. The methodology for deriving the baseline and anomalies for ET, PET, and ESI matches those used for NDVI and precipitation, with a baseline from 2002 to 2012 and drought years of 2013, 2014, and 2015.

Randomization analysis of variance

Mean seasonal NDVI, ET, PET, and ESI raster images were tested for significant differences across land cover types using a one-way, type 1, fixed-effects randomization analysis of variance (ANOVA). The land cover classes include agriculture, grassland, deciduous forest, mature forest and secondary forest (Fig. 2). This analysis uses the Tukey post hoc test (Tukey 1949) to quantify differences within the group of land cover variables and to determine their statistical significance. Note that the Tukey test was developed specifically to account for multiple comparisons and thus a correction for multiple testing is not needed.

The spatial and temporal autocorrelation of the pixels could violate ANOVA assumptions of random sampling and independence. To address this, we randomly selected 1,000 pixels for each land cover category and included only those in the ANOVA, thus reducing the possibility of autocorrelation (Adèr 2008). After randomization, we tested the assumptions of normality and homoscedasticity. Neither of these assumptions were met by the variables (ESI, ET, PET, and NDVI), indicating that the data are not normally distributed nor are they homoscedastic (rejected Shapiro-Wilk test null hypothesis of normality [$P < 0.0001$] and rejected the Bartlett test null hypothesis of homoscedasticity [$P < 0.0001$]). However, we concluded that ANOVA is robust enough to these violations to produce usable results (Adèr 2008).

Time series analysis

Time series decomposition.—The time series decomposition analysis in this study follows the seasonal and trend decomposition procedure (STL) developed by Cleveland et al. (1990). STL decomposes a series into trend, seasonal and remainder components using a locally weighted least squares approach known as LOESS (LOcally wEighted regreSsion Smoother). As a dynamic factor analysis, stationarity of data is not required for STL (Zuur et al. 2003). Therefore, stationarity was not tested until the autocorrelation and partial autocorrelation analysis in the next section.

The seasonal component of an STL decomposition is found by local polynomial regression smoothing of the monthly mean values in the time series. At point x, for instance, the fit is made using points in a neighborhood of x, weighted by their distance from x. This analysis sets the size of the neighborhood by including 75% of the points, and weighted these points with tricubic weighting (proportional to $(1 - (\text{dist}/\text{maxdist})^3)^3$; where dist is the distance between the current point and x and maxdist is the maximum distance between x and all other points in the defined neighborhood. After computing the seasonal values, they were removed from the data, and the remainder was smoothed to find the trend. The overall level was removed from the seasonal component and added to the trend component. This process was iterated twice. The remainder component is the residuals from the seasonal plus trend fit. The source code of the algorithm is *available online*.[8]

This study used an additive rather than a multiplicative time series decomposition model for all of the input variables because no changes in the magnitude of the effects of seasonality were observed in the time series of precipitation, NDVI, ET, PET, or ESI.

Autocorrelation and partial autocorrelation.—We investigated whether there is autocorrelation in the precipitation, NDVI, ET, PET, and ESI time series anomalies by computing autocorrelation and partial autocorrelation coefficients. We computed a monthly climatology by first averaging monthly values for the baseline period of 2002–2012. To derive monthly anomalies, we subtracted the averaged baseline monthly values from the corresponding monthly means of the drought years of 2013, 2014, and 2015.

The autocorrelation function gives the correlation of a time series with its own lagged values and does not control for the values at all shorter lags of the time series. It contrasts with the partial autocorrelation function, which does control for all shorter lags. In other words, the partial autocorrelation is the amount of correlation between a variable and a lag of itself that is not explained by correlations at all lower order lags. The algorithms used to calculate autocorrelation and partial autocorrelation coefficients both fit autoregressive

[6] https://lpdaac.usgs.gov/data_access/
[7] https://ladsweb.modaps.eosdis.nasa.gov/
[8] https://github.com/SurajGupta/r-source/blob/master/src/library/stats/R/stl.R

models of successively higher orders up a maximum lag of $10\log(N/m)$ where N is the number of observations and m the number of series.

We tested for "wide-sense" stationarity (i.e., testing whether the mean and autocovariance vary with respect to time) in the precipitation, NDVI, ET, PET, and ESI time series anomalies using the augmented Dickey-Fuller test and the KPSS test for level stationarity. Both tests agreed that each time series data set was stationary under a threshold of $\alpha = 0.05$ with the exception of the precipitation anomalies time series, which the augmented Dickey-Fuller test suggested was stationary ($P < 0.01$) but the KPSS test suggested that the data were not stationary (reject the null hypothesis of stationarity with $P = 0.0124$). Once we differenced the precipitation anomalies time series by 1 lag, we tested the resulting time series, which was now one month shorter than it was originally, and found that the time series was now stationary. (KPSS null hypothesis of stationarity accepted with $P > 0.1$).

Time series cross-correlation.—To assess the magnitude and significance of temporally lagged relationships between precipitation and the drought response variables of NDVI, ET, and ESI, we used time series cross-correlation analysis. Cross-correlation is a measure of similarity of two series as a function of the displacement of one relative to the other. This analysis enables us to answer the question: Does a change in precipitation transfer to NDVI, ET, or ESI time series several periods later? If so, at which lag is the correlation between two time series strongest?

Uncertainty characterization of remote sensing products

Validation of precipitation and ET data is most often based on comparing data from single gauging stations with remote sensing pixels. Duan and Bastiaanssen (2013) discuss how this approach suffers from the "scale mismatch issue," which arises in the assumption that a single gauging station can be representative of the precipitation of a larger area (Almazroui 2011, Heidinger et al. 2012). Many studies address this scale mismatch by conducting a validation of remote sensing pixels that contain multiple measurement towers and use the mean value as the ground truth for each pixel (Nicholson et al. 2003, Dinku et al. 2007, Chokngamwong and Chiu 2008, Yong et al. 2010). A novel approach for pixel-to-point comparisons proposed by Rammig et al. (2018) determines the statistical properties of "within-pixel" variability and observational errors, and uses this information to correct for their effect when large-scale area averages (pixels) are compared to small-scale point estimates. First, this approach characterizes the global variability of the point data set with the global variance and mean. Then it calculates "within-pixel variability" by analyzing within-pixel covariance, which is equivalent to the sum of variance caused by small-scale variability and observation error in a semivariogram. Global variability is reduced by within-pixel variability to produce a corrected variability measure. Finally, mean and variance of pixels are compared to corrected point mean and variance with statistical measures including mean bias, pattern amplitude, and similarity of pattern.

The network of weather stations from the Costa Rica Instituto Meteorologico Nacional comprises about 13 towers, only 3 of which cover the entirety of the time period of this study. Conducting a validation with only 3 towers would suffer from scale mismatch issues, which could not be addressed by the Rammig et al. (2018) approach due to small sample size. We decided to adopt an error estimate from other validation studies of the TMPA-3B43V7 product that had access to a denser network of weather stations.

Precipitation.—Dinku et al. (2007) conducted an extensive evaluation of 10 different satellite rainfall products using a dense station network over a complex topography in the Ethiopian highlands. Evaluation was for two groups of products. The first group, which TMPA-3B43 falls into, had low spatial (2.5) and temporal (monthly) resolution. In addition to TMPA-3B43, this group included the National Oceanographic and Atmospheric Administration Climate Prediction Center (NOAA-CPC) merged analysis (CMAP) as well as the Global Precipitation Climatology Project (GPCP) multi-satellite and satellite-gauge products. CMAP and TMPA-3B43 performed the best, with a bias < 10% and an root-mean-square error (RMSE) of about 25%. The overall performance of TMPA-3B43 is very good, particularly considering the complex topography of the test region. These results are consistent with results found for West Africa (Nicholson et al. 2003, Ali et al. 2005).

The CHELSA (climatologies at high resolution for the earth's land surface areas) precipitation algorithm incorporates orographic predictors including wind fields, valley exposition, and boundary layer height, with a subsequent bias correction. The resulting data consist of a monthly temperature and precipitation climatology for the years 1979–2013, which does not span the entirety of this study period. Nonetheless, we leverage the Karger et al. (2017) validation to further inform associated error estimate of the TMPA-3B43V7 product used in this analysis. Karger et al. (2017) compare the data derived from the CHELSA algorithm with other standard gridded products including TMPA-3B43, CRU, WorldClim, CHPclim, GPCC, and ERA-Interim and station data from the Global Historical Climate Network. For the spatial comparison, all products evaluated, with the exception of ERA-Interim, showed similar amounts and patterns of biases when compared to validation data. In Costa Rica specifically, the bias ratio was about 1.2, indicating overestimation of precipitation compared to the in situ data.

Evapotranspiration.—Fisher et al. (2009) examined the controls on evapotranspiration in tropical vegetation at 21 pan-tropical eddy covariance sites, conducted an evaluation of 13 evapotranspiration models at these sites, and assessed the ability to scale up model estimates of evapotranspiration for the test region of Amazonia. The radiation-based evapotranspiration models performed best overall for three reasons: (1) the vegetation was largely decoupled from atmospheric turbulent transfer, especially at the wetter sites; (2) the resistance-based models were hindered by difficulty in consistently characterizing canopy and stomatal resistance in the highly diverse vegetation; and (3) the temperature-based models inadequately captured the variability in tropical evapotranspiration.

Across all 21 eddy covariance sites, PT-JPL performed better than all of the other process-based models evaluated (RMSE = 22.8 W/m^2 and R^2 = 0.91). The only model that performed better than PT-JPL was the neural network model (RMSE = 20.6 W/m^2 and R^2 = 0.91) because it was empirically fitted to the point data. The neural network model provided a useful comparison with the more mechanistic models tested. However, when applied to the test region of Amazonia, it resulted in unrealistic values outside of the tower footprint due to its empiricism to the individual sites. PT-JPL, on the other hand, is scalable beyond the eddy flux footprint because it is driven primarily by large-scale parameters including radiation, temperature, and humidity.

Ershadi et al. (2014) examined a number of models including SEBS, PT- JPL, the advection-aridity model of Brutsaert and Stricker (1979) and a single-source Penman-Monteith (PM) model (Monteith 1965), and validated them against a set of twenty flux towers distributed across a range of biome types. Considering overall results, the study found that PT-JPL was the best performing model, followed by SEBS, PM, and advection-aridity. Expanding on the results from tower-scale validations, McCabe et al. (2016) assessed four commonly used evaporation models against data from tower-based eddy covariance observations as well as large-scale globally gridded data distributed across a range of biomes and climate zones. Using surface flux observations from 45 globally distributed eddy covariance stations as independent metrics of performance, the tower-based analysis indicated that PT-JPL provided the highest overall statistical performance (R^2 = 0.72; RMSE = 61 W/m^2).

Results also indicated that the global gridded data tended to reduce the performance for all of the studied models when compared to the tower data, likely a response to scale mismatch and issues related to forcing quality. In the gridded global validation, PT-JPL performed consistently well relative to the other models that have more complex structures and parameterization configurations, with an increase in RMSE of 22 W/m^2. One possible reason for this response that McCabe et al. (2016) suggested relates to the constraint functions of PT-JPL serving a wide range of hydro-meteorological conditions, encompassing energy-limited (e.g., boreal climate) to water-limited (e.g., dry climate) to energy-abundant and water-abundant (e.g., tropical climate) conditions.

Given that the data used in this study were computed with gridded remote sensing products, we apply the error estimates from the gridded validation over the tropics from McCabe et al. (2016) to the PT-JPL ET and PET data used here, with RMSE = 83 W/m^2 and R^2 = 0.48.

Potential evapotranspiration.—Maes et al. (2018) compare the performance of the 15 most common methods for computing PET. The study used eddy covariance measurements from 107 sites of the 10 FLUXNET2015 database, covering 11 different biomes, to parameterize and compare these methods and uncover their relative performance. For each site, Maes et al. (2018) extracted the days for which ecosystems are unstressed based on both an energy balance approach and on a soil water content approach. The validation of the 15 PET estimation methods used the unstressed days as the ground truth to reference.

The results indicate that a simple radiation-driven method calibrated per biome consistently performed best, with an unbiased RMSE of 0.56 mm/d and a bias of −0.02 mm/d against in situ measurements of unstressed evaporation. The Priestley and Taylor method that did not calibrate per biome performed slightly worse. Yet it performed substantially and consistently better than more complex Penman, Penman-Monteith-based, or temperature-based approaches with an overall unbiased RMSE of 0.75 mm/d and bias of 1.14 mm/d. Focusing in on the results for biomes found in Guanacaste, including deciduous broadleaf forest, mixed forest, and woody savanna, the accuracy slightly decreases compared to the overall accuracy measures of uncalibrated Priestly and Taylor PET estimates: unbiased RMSE of 0.76 mm/d and bias of 1.27 mm/d).

Results

Spatial anomalies of precipitation and NDVI

The entire region of Guanacaste experienced negative anomalies of precipitation in the wet seasons of 2013, 2014, and 2015 (Fig. 4). Drought severity intensified over these three years, with 2015 experiencing the most negative precipitation anomalies, reaching about −175 mm in the eastern region of the province and about −125 mm in the coastal, western region. Correspondingly, NDVI tended to be below average during the wet seasons of 2013, 2014, and 2015, with 2014 seeing the largest decreases (Fig. 4). However, in the southwestern portion of Guanacaste, NDVI anomalies were negligible or even slightly positive despite low rainfall.

Analysis of a 64-yr precipitation record containing averaged GPCC and MPA-3B43V7 products yielded a wet season SPI of 2015 of −3.46, the lowest 6-month SPI in the historic record. This followed wet season SPI of −2.80 in 2014 and −1.14 in 2013. Other recent

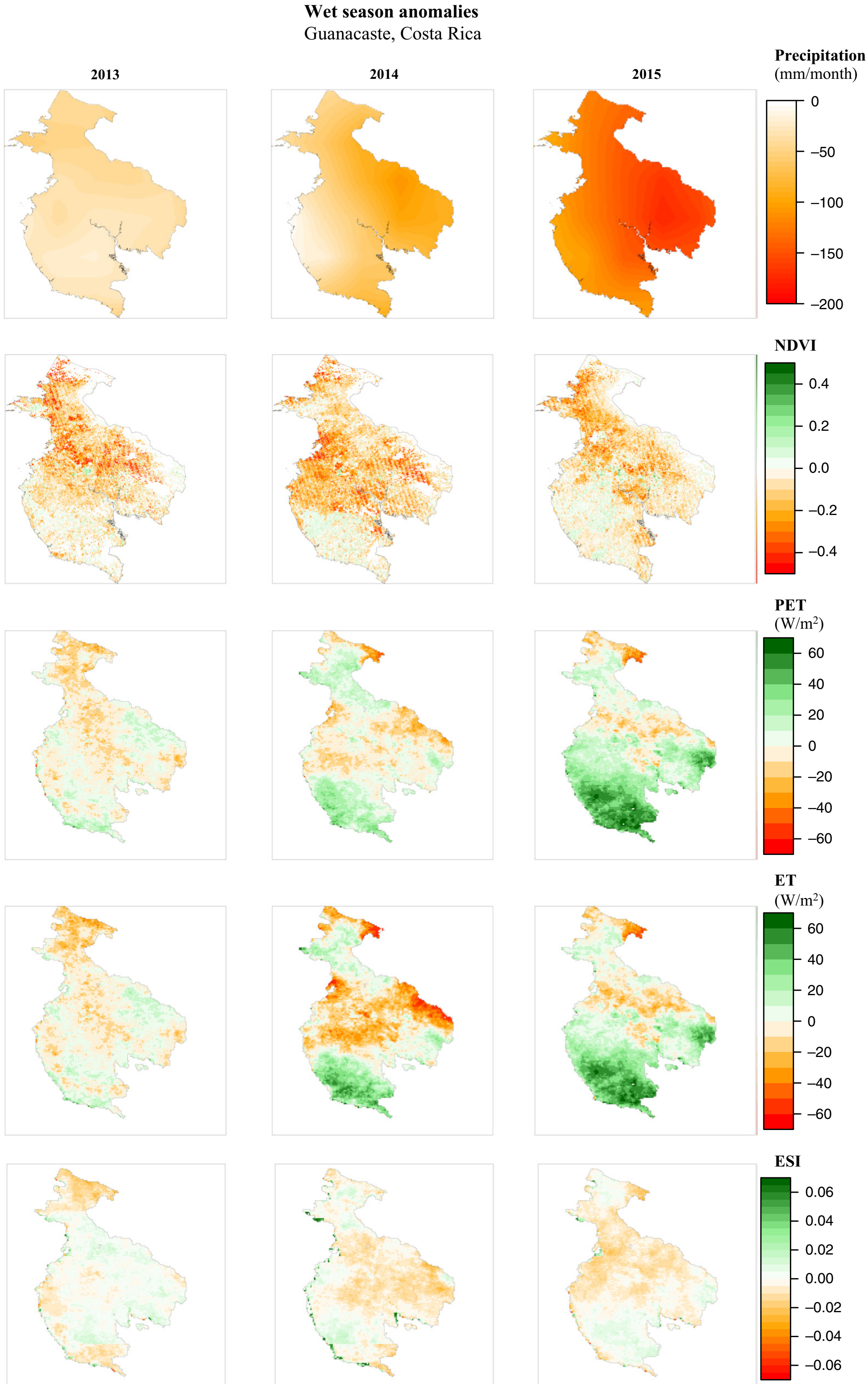
Wet season anomalies
Guanacaste, Costa Rica
2013
2014
2015
Precipitation
(mm/month)
0
−50
−100
−150
−200
NDVI
0.4
0.2
0.0
−0.2
−0.4
PET
(W/m²)
60
40
20
0
−20
−40
−60
ET
(W/m²)
60
40
20
0
−20
−40
−60
ESI
0.06
0.04
0.02
0.00
−0.02
−0.04
−0.06

FIG. 4. Wet season anomalies of five hydrologic and drought indicators, including precipitation, NDVI, ET, PET, and ESI across three years of record (2013–2015) compared to the baseline (2002–2012). The year of 2015 stands out with the lowest negative mean wet season precipitation anomalies compared to the other drought years of 2015, 2014, and 2013. However, vegetation stress as measured by NDVI, ET, and ESI anomalies is not highest in 2015 compared to the other two drought years.

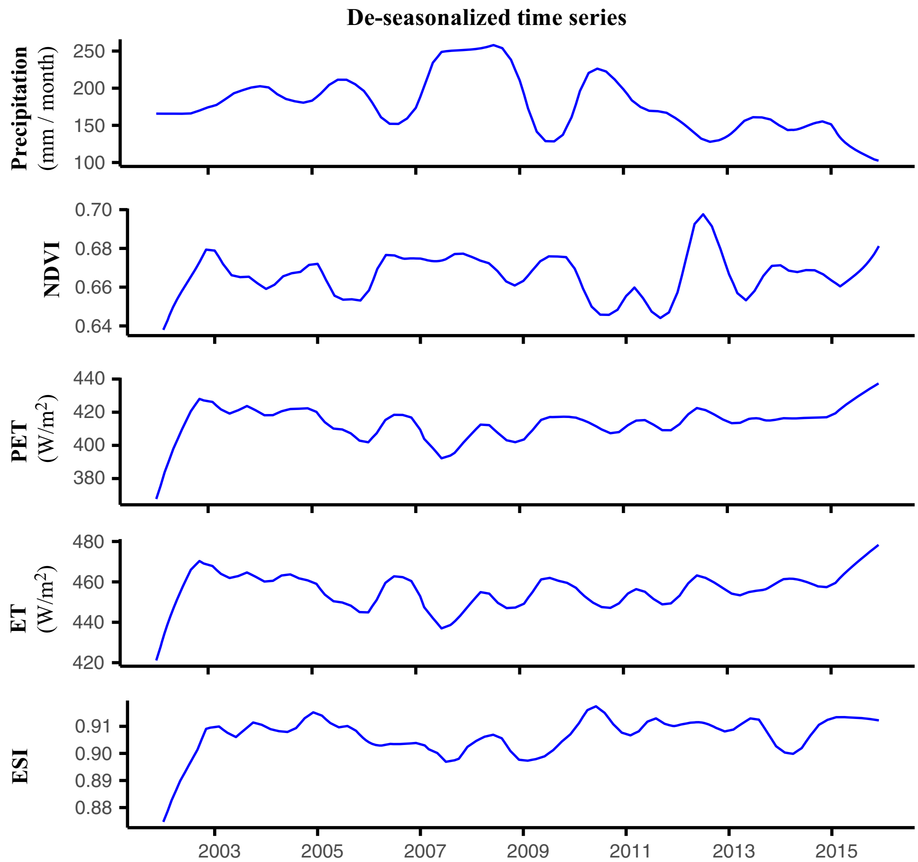

FIG. 5. The smoothed (de-seasonalized), low-frequency trend component of the time series decomposition of monthly precipitation, NDVI, ET, PET, and ESI time series spanning 2002–2015. The de-seasonalized trend component has the same units as the original data series. Even though 2015 has the steepest decrease in precipitation trend compared to the other drought years, that year shows higher NDVI, ET, and ESI values than 2014, suggesting that vegetation stress may have decreased from 2014 to 2015.

drought events took place in 2006–2007 and 2009–2010 (Fig. 5). Furthermore, Guanacaste has seen an increase in the magnitude of precipitation extremes in recent years. The standard deviation of SPI between 1951 and 1999 is 0.73. In contrast, the standard deviation in the time period of 2000 to 2015 is 1.52, which is more than twice the standard deviation observed from 1951 to 1999.

Spatial anomalies of evapotranspiration (ET), potential ET (PET), and evaporative stress index (ESI)

PET tended to be elevated during the 2013 to 2015 drought periods, particularly in the southern portions of Guanacaste (Fig. 4). This is likely due to warmer near-surface air temperature driven by increased net radiation. However, the central region saw little change or even a decrease in PET. PET anomalies were largest in 2015, the year with the most severe precipitation shortages. ET anomalies closely tracked those of PET, with areas of elevated PET seeing elevated ET and areas of below average PET seeing below average ET. However, the evaporative stress index still shows indications of elevated water stress (lower ESI), particularly in the central portion of Guanacaste and generally corresponding to areas that had negative anomalies in NDVI. Even in these areas, ESI anomalies indicate only weak water stress (average values remaining close to 1.0) during the wet season in spite of severe precipitation shortages. Furthermore, the southernmost portion of Guanacaste had some areas showing reduced water stress (elevated ESI) during these periods, corresponding to areas with negligible or even slightly positive NDVI anomalies.

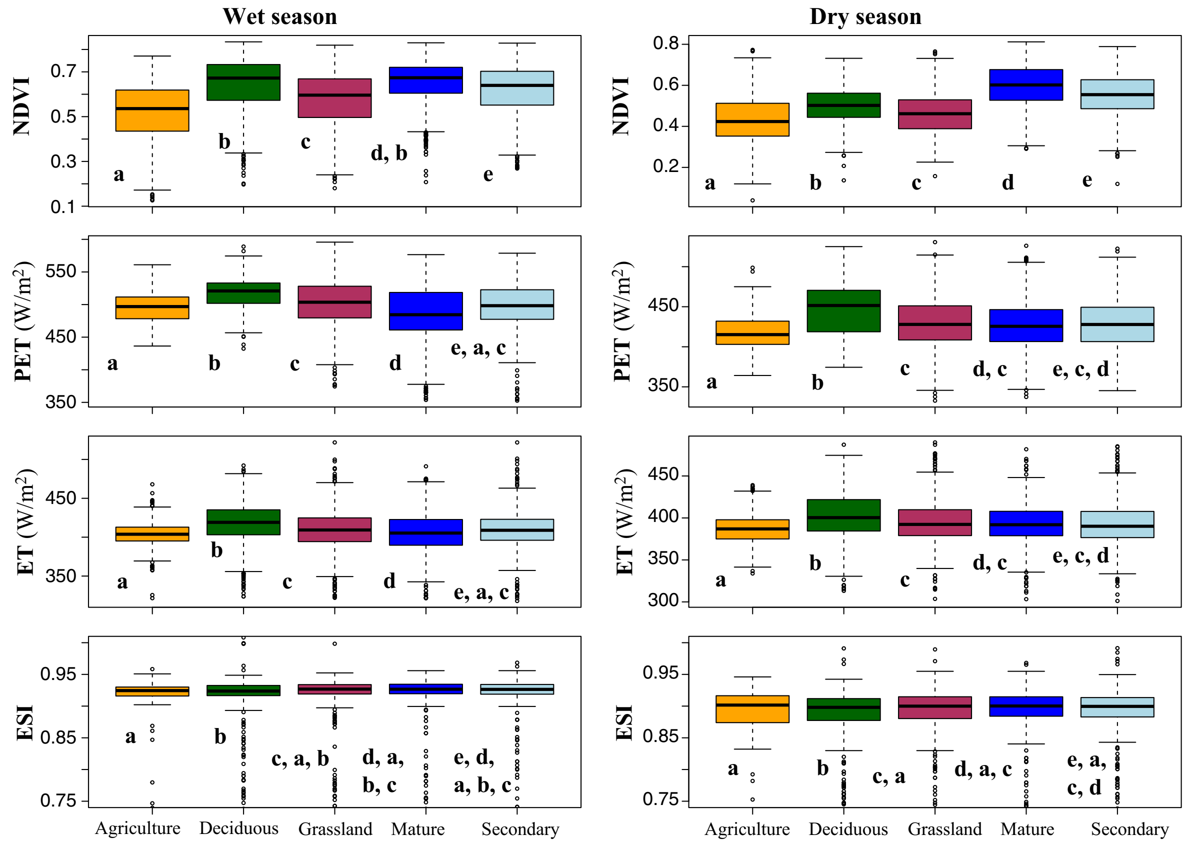

FIG. 6. Box plots of drought indicators of NDVI, ET, PET, and ESI across land cover types for the wet season (left) and dry season (right) in 2015. The letter by each boxplot represents significant differences between land cover groups (with alpha threshold of 0.05), where groups sharing the same letter do not have a statistically significant difference. Box plot components are midline, median value; box edges, 25th percentile (lower quartile) and 75th percentile (upper quartile); upper whisker = min(max(x), Q_3 + 1.5 × IQR), where x is the set of data values, Q_3 is the upper quartile and IQR is the interquartile range; upper whisker = max(min(x), Q_1 + 1.5 × IQR); and points, outliers.

Time series analysis

Time series decomposition.—The seasonality of the precipitation time series shows a dip that takes place in the middle of the wet season during July and August (Appendix S1: Fig. 1). This pattern characterizes the midsummer drought phenomenon, which occurs throughout Central America (Maldonado et al. 2016). The seasonal curve of precipitation shows the midsummer drought followed by a larger spike of precipitation in the second part of the wet season, ending in late October or early November. ET and PET show midsummer dips as well. The seasonal ESI series shows the maximum spike in the beginning of the wet season while the highest point in NDVI occurs in the later part of the wet season. Nonetheless, the signal of the midsummer drought is still picked up within each of the time series.

Removing seasonality from the time series yields a low-frequency, de-seasonalized trend component of precipitation (Fig. 5). The trend shows a sharp decline in 2009 followed by a sharp increase in 2010. Between 2001 and 2015, a gradually declining trend emerges, culminating in an all-time low at the end of 2015. Averaged together over all of Guanacaste, the indicators of vegetation stress (NDVI, ET, ESI) show very little change in trend throughout the most recent drought period of 2013, 2014, and 2015. In particular, even though 2015 has the steepest decrease in precipitation trend compared to the other drought years, that year shows higher NDVI, ET, and ESI values than 2014, suggesting that vegetation stress may have decreased from 2014 to 2015.

Autocorrelation and partial autocorrelation.—The wet season months (May through October) have the highest NDVI, ET, and ESI values, indicating lower vegetation stress during this time of the year (Appendix S1: Fig. 2). The wet season months also typically have the greatest variability in values, suggesting that it is more difficult to characterize these months compared to the dry season. An exception to this arises in the ESI time series, which shows more variability in the dry season. We might expect, therefore, that autocorrelations of smaller lags will not be as large or significant as fourth-, fifth-, sixth-, or seventh-order lags.

Table 2. The one-way randomization ANOVA model output testing for differences in drought response (including normalized difference vegetation index [NDVI], evapotranspiration [ET], potential evapotranspiration [PET], and the evaporative stress index [ESI]) across land cover types for the wet season and the dry season.

Land cover types	SS	df	*F*	*P*	Effect size
NDVI					
Wet season					
Land cover	10.90	4	214.3	<0.0001	0.148
Residuals	62.36	4,906			
Dry season					
Land cover	17.54	4	433.3	<0.0001	0.2576
Residuals	50.54	4995			
PET					
Wet season					
Land cover	520,164	4	147.8	<0.0001	0.1058
Residuals	4,395,135	4995			
Dry season					
Land cover	405,454	4	126.2	<0.0001	0.0917
Residuals	4,012,020	4995			
ET					
Wet season					
Land cover	113,310	4	54.37	<0.0001	0.0417
Residuals	2,602,586	4995			
Dry season					
Land cover	100,485	4	44.87	<0.0001	0.0347
Residuals	2,794,616	4991			
ESI					
Wet season					
Land cover	0.015	4	3.626	0.0059	0.003
Residuals	5.105	4995			
Dry season					
Land cover	0.024	4	5.007	<0.0001	0.0039
Residuals	5.984	4992			

Notes: Each observation is a pixel randomly selected from the study area such that 1,000 pixels were selected per land cover class.

The anomalies of the precipitation time series have the largest significant autocorrelation compared to the other time series anomalies, with the first lag having a correlation of about −0.4 (Appendix S1: Fig. 3). The 13th lag is also above the 95% confidence interval, with a correlation of about 0.2. ESI has a positive and significant correlation with the 15th lag of 0.16. Similarly, the 15th lag of ET is also one of the highest in the time series, with a correlation of similar magnitude but slightly below the 95% confidence interval. The first lag barely passes the 95% confidence interval, with a value of about 0.16.

The impact of controlling for the previous lags in the time series as illustrated in the partial autocorrelation results (Appendix S1: Fig. 4) is not very large. For precipitation, the first, second, and third lags are significant and each have a correlation <−0.25. The 12th lag becomes significant and is also negatively correlated, though smaller in magnitude compared to the first, second, and third lags. None of the lags in NDVI, ET, PET, and ESI anomalies plots are notably large or significant, with the first lag having a consistently relatively large value compared to the others in the time series for each variable, but only the first lag of ET passes the 95% confidence interval.

Time series cross-correlation.—Results point to the possible temporal decoupling between precipitation deficits and the impacts of vegetation stress as measured by NDVI, ET, and ESI. For instance, precipitation is lowest in 2015 but NDVI and ESI are lowest in 2014 (Figs. 4 and 5). ET and PET (and thus ESI) are assessed with the PT-JPL model, which could indicate that the lack of negative anomalies in 2015 in ET arose from increased incoming solar radiation as opposed to a response to reduced precipitation. Deciduous forests do not show a response to the drought period, at least not within the time period of this study. Therefore, drought impacts on the landscape in Guanacaste likely comprise temporally lagged responses to the precipitation deficit, suggesting that the drought response in Guanacaste does not fit into Scenario A (immediate increase in vegetation stress) of the conceptual framework for drought assessment. Instead, the drought response might more closely resemble Scenario B (lagged response), in which drought effects of 2013, for instance, propagate several months or even multiple years later in 2014 and 2015. If statistically significant cross-correlations occur, then this indicates that the full effects of the 2015 drought may not impact the vegetation on the landscape until several

TABLE 3. Results from the Tukey post hoc test showing the pairwise differences and significance of the ANOVA terms across land cover types for NDVI, ET, PET, and ESI in (a) the wet season and (b) the dry season.

	Difference			
Land cover types	NDVI	PET	ET	ESI
a) Wet season, 2015				
Deciduous forest–agriculture	0.1198†	22.4067†	13.8222†	−0.0052**
Grassland–agriculture	0.0541†	6.2635†	4.5521†	−0.0022
Mature forest–agriculture	0.1294†	−8.6794†	1.7958	−0.0012
Secondary forest–agriculture	0.0982†	2.9223	5.1925†	−0.0021
Grassland–deciduous forest	−0.0657†	−16.1432†	−9.2701†	0.0020
Mature forest–deciduous forest	0.0095	−31.0861†	−12.0264†	0.0029
Secondary forest–deciduous forest	−0.0215†	−19.4843†	−8.6297†	0.0031
Mature forest–grassland	0.0753†	−14.9429†	−2.7562	0.0010
Secondary forest–grassland	0.0441†	−3.3411	0.6404	0.0002
Secondary forest–mature forest	−0.0311†	11.6017†	3.3967***	−0.0008
b) Dry season, 2015				
Deciduous forest–agriculture	0.0723†	27.4692†	16.7231†	0.0460†
Grassland–agriculture	0.0391†	13.9988†	9.6195†	0.0660
Mature forest–agriculture	0.1644†	10.4471†	7.3860†	0.0384
Secondary forest–agriculture	0.1228†	12.0975†	6.9269†	0.0201
Grassland–deciduous forest	−0.0332†	−13.4703†	−7.1035†	0.0276
Mature forest–deciduous forest	0.0921†	−17.0221†	−9.3371†	0.0076†
Secondary forest–deciduous forest	0.0505†	−15.3716†	−9.7961†	0.1063†
Mature forest–grassland	0.1253†	−3.5517	−2.2335	0.0118
Secondary forest–grassland	0.0837†	−1.9012	−2.6925	−0.0024
Secondary forest–mature forest	−0.0416†	1.6504	−0.4590	0.0152

$^{**}P < 0.01$; $^{***}P < 0.001$; $^{†}P < 0.0001$.

months or years later. To test this, we conducted a cross-correlation analysis between precipitation and NDVI, ET, PET, and ESI anomalies, where significantly correlated lags of precipitation in vegetation stress indicators would suggest a lagged response to precipitation anomalies. If none of the lags from the cross-correlation analysis are significant, then Scenario C (no response) would best characterize the regional drought response.

The cross-correlations between raw precipitation and NDVI, ET, PET, and ESI all clearly reflect the seasonal pattern of each series and support the hypotheses stated above (Appendix S1: Fig. 5). The statistically significant correlations for NDVI, ET, and ESI start with positive correlations at lags 0 through −2 and negative correlations at lags −7 through −10, followed by positive and still statistically significant three-month lags for the previous year, followed by negative statistically significant three-month lags, etc. The cyclical positive correlations support the assessment that the peak period for low vegetation stress (high NDVI, ET, and ESI) occurs around two months after the start of the wet season and high vegetation stress is expected around two months after the start of the dry season. The cyclical negative correlations support the hypothesis that there are two periods each year in which changes in precipitation have not caught up with changes in vegetation.

Results indicate that PET leads precipitation by a couple months in the wet season (lag 1 is the peak correlation) as well as the dry season (lag 7 is the lowest correlation). This could arise because, as suggested in the hypothesis, in the end of spring and beginning of summer, temperatures rise but precipitation has not peaked, meaning that there is less cloud cover, allowing for optimum solar radiation. As the wet season progresses, there are slightly higher temperatures but also larger amounts of precipitation, particularly the second precipitation peak, which typically occurs in September. Similarly, in the beginning of the dry season, there are still some high temperatures with lower cloud cover. However, as temperatures drop, net radiation also drops, even with almost no cloud cover.

For the anomalies time series cross-correlations (which controls for the baseline by subtracting monthly mean values between 2002 and 2012 from each corresponding month of the time series), we hypothesized a similar set of relationships as those described for the raw data, with the exception of having more noise in the results as well as potentially longer lag periods. When strictly looking at anomalies, we still expected to see positive correlations between precipitation anomalies and NDVI, ET, and ESI anomalies. Increases in precipitation are associated with lagged increases in NDVI, ET, and ESI several lags later and decreases in precipitation are associated with lagged decreases in NDVI, ET, and ESI several lags later.

The cross-correlations between precipitation anomalies and NDVI anomalies follow a seasonal pattern described in the hypothesis, though this pattern is less distinct as the cyclical pattern in the raw cross-correlation results (compare Appendix S1: Fig. 4 with Fig. 7). The cross-correlations for NDVI were mostly negative close for lags close to 0, positive from lags −8 to −12, negative from −14 to −18, positive from −23 to −26, negative from −33 to −38, and positive from −43 to −46, with typically one lag within each range passing the 95% confidence interval. A similar pattern but with less regularity and fewer cases of significance arises in the ET time series. This finding supports our hypothesis that increases in vegetation stress as measured by decreases NDVI and ET is detected around the initial months with increases in precipitation. And, vice versa, decreases in vegetation stress around the beginning months with decreases in precipitation in the dry season.

ESI, in contrast, has positive correlations for lags close to zero (although they are not quite significant) and negative correlations for lags between −4 and −7. A possible reason why we did not see ESI cross-correlations match NDVI and ET could be because vegetation in Guanacaste typically is able to match changes in atmospheric demand regardless of changes in precipitation. The similar cross-correlation graphs of ET and PET support this possibility. Lags in the plot of PET and precipitation have significant negative correlations for lags from 0 to −3 and positive (but not quite significant) correlations for lags −8 through −11, which supports our initial hypothesis of lagged impacts of seasonality.

Randomization analysis of variance (ANOVA)

In both the wet season and the dry season of 2015, grasslands and agriculture generally experienced statistically significantly lower ET and NDVI compared to forest land cover classes, particularly deciduous forest type (Table 2, Table 3, Fig. 6). ESI was close to 1.0 during the wet and dry season (typically between 0.85 and 0.95) during 2015, indicating a general lack of water stress. Differences in ESI values were very small and not statistically significant across any combination of land cover categories, with the exception of deciduous forest and agriculture: agriculture had significantly higher ESI compared to deciduous forests, especially in the dry season (compare Table 3a with Table 3b). This result could be explained by the availability of irrigation to most agricultural fields in Guanacaste.

Discussion

Drought assessment in Guanacaste

Meteorological drought events (SPI < −1.0) occurred in 2013, 2014, and 2015, with 2015 seeing the most extreme shortage in a 64-yr historical record. Precipitation shortfalls were most pronounced in the eastern portion of Guanacaste, but extended across the entire region (Fig. 4). It is therefore surprising that ET was impacted with only subtle reductions during the drought years, and even increasing in the entirety of southwestern Guanacaste during the 2015 wet season. Similarly, the evaporative stress index (ESI) showed only modest increases in ecosystem water stress during any of the drought years. Reductions in ESI are at most 0.03 and more often are about 0.015, which shows a reduction in ET relative to PET of only 1.5%. In terms of magnitude, this result is almost negligible. Therefore, during the drought years, the majority of Guanacaste showed either small changes or no changes in vegetation stress as measured by ESI, which indicates that vegetation drought response in the province as measured by ESI most closely follows Scenario C in the conceptual framework of drought assessment, at least in the short term. On the other hand, NDVI showed overall decreases in all three drought years in most of Guanacaste. This most closely resembles a Scenario A response.

Precipitation deficits often occur simultaneously with high solar radiation, high temperature, and low air humidity, all of which drive increases in PET (Shah and Paulsen, 2003, Vicente-Serrano et al. 2013). The results from this analysis mostly show the same relationship: the year with the largest decrease in precipitation also experienced the largest increase in PET over the entire province (even though the largest increase in PET occurred in the region with the smallest decrease in precipitation for that year). In contrast, decreases in rainfall are often associated with decreases in ET, because when plants are water stressed, they try to conserve water by closing their stomata, causing the transpiration component of ET to decrease (Anderson et al. 2007, Fisher et al. 2011). The characteristic decrease in ET as a result of negative precipitation anomalies did not occur in Guanacaste; in fact, ET actually tracked the large increases in PET in the southwestern region. It is possible that even if plants decrease their conductance to water vapor as a response to the 2015 drought (i.e., decrease the transpiration component of ET), the evaporation component of ET increased enough to compensate for the decrease in transpiration allowing for ET to keep up with the increases in PET.

One explanation for why ET and ESI did not decrease throughout Guanacaste as much as might be expected is the region's sub-humid climate with abundant precipitation. This may have buffered plants from the full effects of the large precipitation deficits. The region has an average annual rainfall of about 1,691 mm, with about 82.2% air humidity in the wet season and 67.8% air humidity in the dry season. Even with several months of precipitation shortages averaging 150 mm in 2015, there is still about 1,000 mm of rainfall over the year, and it may have been enough to keep up with evaporative demand throughout the drought years.

Another possible reason for the modest decreases in ET and ESI involves the availability of other sources of water. The lack of notable decreases in ET and ESI anomalies in the agricultural areas likely occurred due to an increase in irrigation: unlike other areas in the dry corridor, Costa Rica has access to infrastructure and funding that allow water to divert from the wet, Atlantic region to agricultural fields on the dry, Northwestern Pacific region of Guanacaste (Jiménez et al., 2001). Furthermore, vegetation may have access to shallow groundwater in the region. This could explain why vegetation, particularly in grassland and forest ecosystems in southeastern Guanacaste, may have been able to continue to match ET with atmospheric demand (PET) even with the large increases in PET the during 2015 in the southwestern portion of Guanacaste.

The southwestern part of Guanacaste experienced the smallest decrease in precipitation compared to the other areas of the province in 2015, with the difference in anomalies from east to west equal to about 50 mm. These wetter conditions in the southwestern region may have enabled plants to continue to meet elevated evaporative demand with increased transpiration. However, given that the wet season anomaly was still about 125 mm per month below the baseline in the southwestern part of Guanacaste, it is possible that the drought-resilient characteristics of the primarily deciduous forest ecosystem in that region (Fig. 2) also contributed to the region's ability to maintain NDVI values as well as increase ET to match PET. Trees tend to have deeper roots than grasses growing in grassland ecosystems, providing greater access to water in the subsurface. The vegetation in the forested region continued to meet atmospheric demand, suggesting that the forest may be drought resilient enough to withstand the impacts of the most severe drought conditions in the past 64-yr record, at least in the short term. This response is somewhat similar to that of Amazon forests responding to short-term drought in 2005 (Saleska et al. 2007), whereby forests exhibited a green-up in spite of drought. Saleska et al. (2007) attribute the observed green-up to increased availability of sunlight due to decreased cloudiness. This could be one explanation for the pattern mirrored by the results of this study, where NDVI declines during the drought years but not for the mostly deciduous forest land cover type in the southwest of the province.

The lack of change in the spatial anomalies of NDVI and ESI suggests that no major changes in vegetation stress occurred in the southwestern part of Guanacaste, resembling Scenario C in the drought assessment framework. However, for most of Guanacaste, the NDVI anomalies depict Scenario B (increase in vegetation stress) in the conceptual framework while ESI depicts Scenario C (no increase or decrease in vegetation stress). The difference in conceptual scenarios for indices of NDVI and ESI highlights the decoupled responses of the respective indices. However, the decoupling observed here differs from findings of other studies: as an early warning sign of drought, ESI often declines before NDVI because plants typically close their stomata and conserve water before any detectable changes in greenness occur (Anderson et al. 2011).

The two possible explanations provided as to why ESI did not decrease as much as expected in most of Guanacaste point to the sub-humid climate in Guanacaste and to other sources of water availability. However, if those two phenomenon were responsible for the lack of drought impacts as measured by ESI, then it is likely that NDVI would also show a similar lack of response as ESI. If vegetation was able to match atmospheric demand, then NDVI would not be expected to decrease. Similarly, if there was shallow groundwater available, then this would also be reflected in NDVI. But instead NDVI anomalies were strong and negative in most of the study area across all drought years. The large differences in assessments about vegetative drought response conveyed by NDVI and PT-JPL-derived ESI anomalies could prompt further investigation of PT-JPL in terms of how well it captures regional changes in drought response. Fisher et al. (2008) validated PT-JPL across a wide range of climates and plant functional types with success (RMS = 16 mm/month or 28% for 16 eddy covariance tower sites across two years). Nonetheless, it is possible that PT-JPL did not effectively capture the regionally specific variation and nuances in the relationship between ET and PET. For instance, PT-JPL uses a greenness measure (NDVI) to constrain PET and derive ET estimates. While strong empirical correlations between NDVI and vegetation biomass generally exist across broad gradients, greenness lacks localized information on vegetation structure and function, both of which play important roles in determining regional vegetative ET response to drought conditions (Houborg et al. 2015).

Implications for land management practices and environmental decision making

An implication of this research is that land managers have an opportunity to steward resources in a way that reflects the understanding that their decisions can improve (1) the efficiency of current "business as usual" irrigation practices and (2) the underlying land stewardship strategy so that it is more drought resilient.

The 1-km data used in this study fit a regional analysis of drought but are too coarse for agricultural irrigation applications. Obtaining high-resolution estimates of ET represents a cost-effective way to detect intra-field variability of plant stress, which can help agriculturalists apply precise irrigation methods based on crop requirements (Melton et al., 2012). Under the crop coefficient FAO-56 approach (Allen et al. 1998), which depends on measuring plant ET capacity, ET data can help to identify the quantity and timing of water additions needed to avoid stress as operations aim to optimize limited water resources. Such localized studies require finer spatial and temporal resolution ET data than those used in this study. The data must be accessible and have global coverage to enable adoption from ecologically and economically diverse stakeholders (Reid and Oki 2014). Many of these stakeholders otherwise could not afford the financial and time costs associated with in situ data collection but would benefit from using the data to optimize water use. With the launch of NASA's ECOsystem Spaceborne Thermal Radiometer Experiment on Space Station (ECOSTRESS) in June 2018, ECOSTRESS provides ET

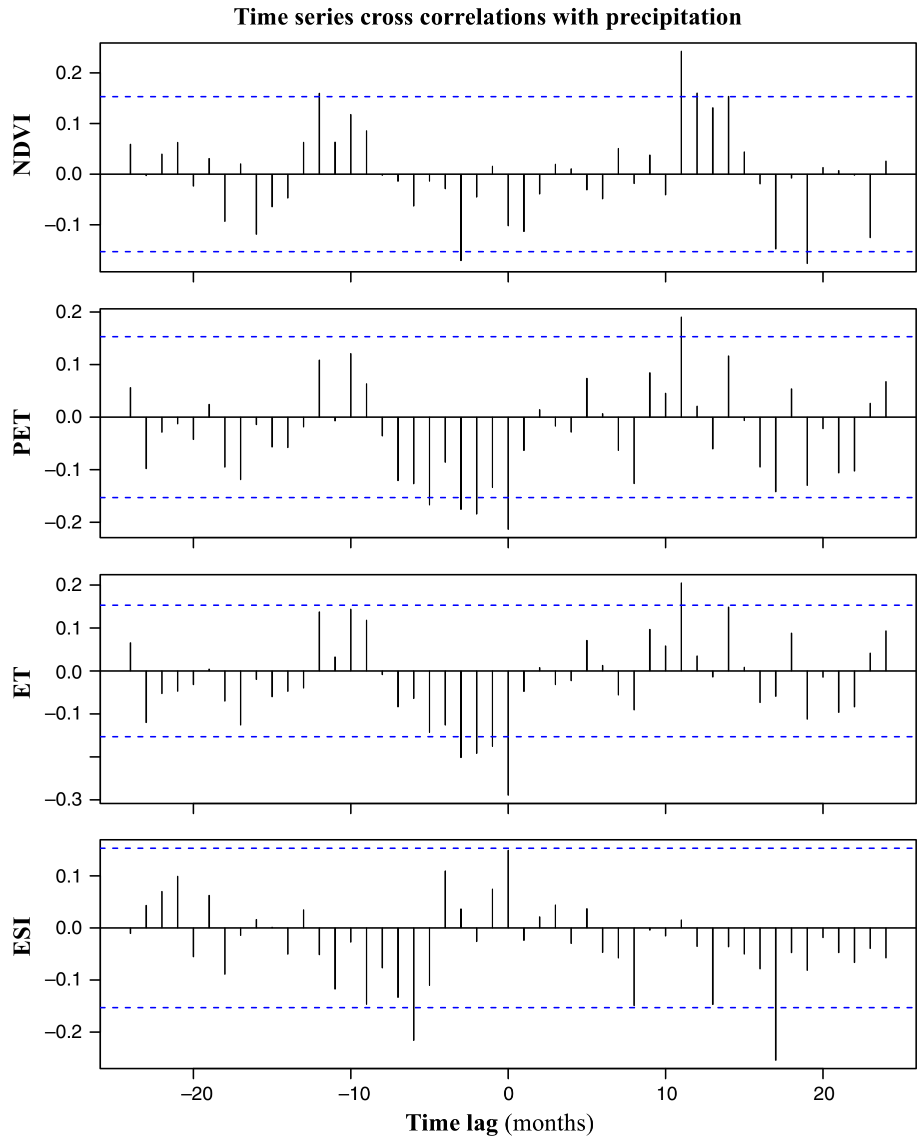

FIG. 7. Results from the time series cross-correlation analysis for 24-month lag period between precipitation anomalies and NDVI, ET, PET, and ESI anomalies spanning 2002–2015. The cross-correlations between precipitation anomalies and NDVI anomalies follow a seasonal pattern. This pattern arises in the PET and ET time series but with less regularity and fewer cases of significance.

at 70-m pixel resolution approximately every four days, which will help resolve spatial and temporal gaps in the current approaches to studying vegetation stress using Landsat (low temporal resolution) and MODIS (low spatial resolution) data. At such spatial scales, opportunities arise for providing ET-based irrigation recommendations as well as identification of drought-resilient crop varieties (Tuberosa and Salvi 2006).

In addition to making business as usual agricultural irrigation and crop variety selection more efficient, a potentially more promising implication of this research that we hope future studies explore involves supporting a shift in the fundamental agricultural land management practices such that they become more drought resilient. This shift is particularly urgent in the context of increased intensity, frequency and duration of extreme drought conditions predicted to result from increased greenhouse gas emissions. Determining which natural and managed ecosystems are most vulnerable to vegetation stress, and their time scales, can support forecasting of drought effects and subsequent decision making around land and water resource management. For Guanacaste in particular, Kuzdas et al. (2015) assert the need for "transformational change" in water governance, indicating that increases in efficiency alone are not sufficient for creating sustainable and drought resilient water use in Guanacaste. More fundamental and systemic changes in natural resource stewardship are necessary.

Lower ET values in grasslands and agriculture compared to deciduous forest might result from lower soil moisture retention, a less regulated microclimate, and shallower root systems with less extensive access to deep water. It is difficult to predict how ET and NDVI would change if PET increased uniformly in every part of Guanacaste the way it did in the southwestern region. One possibility is that only the forested region would be able to meet the increase of PET with a proportional increase in ET. In particular, the ecosystem that would likely suffer the most in terms of plant stress would be grassland due to the lack of root depth for accessing moisture deeper than the shallowest root zone as well as a less regulated microclimate (Lin 2007). In the agricultural regions of Guanacaste, most of which have access to irrigation, ET would likely be able to rise the same amount as PET. In the absence of irrigation, however, the conventional monocrop agriculture systems of the province may have experienced plant stress resembling grasslands in Guanacaste. The recent drought in the Dry Corridor caused countries that lack irrigation to fall victim to water shortage and crop failure, which in turn decreased food security, jeopardized safety, and threatened livelihoods (United Nations Office for the Coordination of Humanitarian Affairs 2014, 2016).

The drought response of deciduous forest ecosystems in Guanacaste consistently showed significantly lower vegetation stress across NDVI, ET, and ESI compared to grassland, at least in the short term. Therefore, one approach for agriculture to become more drought-resistant involves transitioning from large monocrop fields, which are similar to grasslands in terms of structure, into systems that emulate forest ecosystems, which have drought-resilient characteristics such as increased biodiversity, more mild microclimates and deeper roots compared to grassland (Lin 2007, Tscharntke et al. 2011).

Shade-grown coffee represents one example of drought-resilient agricultural land management. The study conducted by Lin (2010) examines the ability of shade trees to maintain water availability for coffee in a shade agroecosystem in Southern Mexico. Soil evaporation and evaporative demand for crop transpiration were compared in coffee systems under different levels of shade canopy during both the wet season and dry season between July 2004 and June 2005. With 60–80% shade cover, daily soil evaporation rates significantly decreased by 41% compared to the low shade site (10–30% shade). Furthermore, coffee transpiration demand was strongly affected by shade cover as shade cover impacts microclimate factors including light, temperature, and air saturation vapor pressure deficit. Shade cover above 30% showed significant reductions of 32% in evaporative demand when compared to the low shade site. Linn (2010) concludes that the presence of shade cover in agroforestry systems is capable of reducing overall evaporative demand from soil evaporation and transpiration, therefore offering a higher level of crop protection for farmers with agricultural vulnerability to reduced water resources.

Additional benefits associated with shade trees in agroforestry include enhancement of functional biodiversity, carbon sequestration, soil fertility, as well as weed and biological pest control (Tscharntke et al. 2011). Higher pest densities can result from physiological stress in unshaded cropland. Risk-averse farmers avoid long-term vulnerability of their agroforestry systems by keeping shade as an insurance against insect pest outbreaks. Furthermore, shade-grown coffee systems provide habitat for birds and other animals that prey on pests in the coffee plantations. This greatly reduces the need for pesticide spraying. Decreased or complete elimination of pesticide application creates a positive feedback loop in which improved water quality and ecosystem health protects functional agrobiodiversity such as antagonists of pests and diseases, as well as pollinating bees, which further enhances coffee yield and reduces the need for fertilizer application (Tscharntke et al. 2011).

Conclusion

This study found that vegetation in some parts of Guanacaste was modestly stressed by severe precipitation shortages in 2013, 2014, and 2015. Most of the region had negative anomalies in NDVI, but anomalies in evapotranspiration and evaporative stress index (ET/PET) were surprisingly small. We found almost no vegetation stress in the southwestern forested region of Guanacaste, which may have resulted from smaller precipitation shortfalls coupled with forest ecosystem characteristics such as a more regulated microclimate and more deeply rooted vegetation. Overall, this study illustrates how incorporating ET into a drought assessment can provide information that complements other vegetation metrics such as NDVI. Possible implications of this research and future applications of ET data for agricultural land management and environmental decision-making include guiding irrigation practices and crop variety selection to become more efficient. These implications improve "business as usual" practices, meaning that they reduce the impact of unsustainable practices such as excessive fertilizer runoff (Tscharntke et al. 2011) and over withdrawal of groundwater (Famiglietti et al. 2011, Chen et al. 2014, Iqbal et al. 2016). Another possible implication of this research points to the opportunity to reevaluate conventional agricultural land management practices in pursuit of stewarding managed landscapes such that they are sustainable and drought resilient by design. We explore this with an example that compares the benefits associated with shade-grown coffee vs. conventionally grown coffee. As finer spatial resolution ET data become increasingly available, applications of ET information can continue to help identify drought-resilient ecosystems. The more we learn from these natural systems, the greater potential we have for reimagining what it takes to create drought resilience within managed agricultural systems.

Acknowledgments

We thank the ECOsystem Spaceborne Thermal Radiometer Experiment on Space Station (ECOSTRESS) Mission Applications and the Clark University Edna Bailey Sussman fund for funding this research. We thank Gil Pontius and Ron Eastman for their valuable comments. We also thank Crisman Cooley for sharing his expertise in concise scientific writing and providing helpful edits to this manuscript. The research was carried out at the Jet Propulsion Laboratory, California Institute of Technology, under a contract with the National Aeronautics and Space Administration. Government sponsorship acknowledged.

Literature Cited

Adèr, H. J. 2008. Advising on research methods: a consultant's companion. Johannes van Kessel Publishing, Huizen, Netherlands.

Ali, A., A. Amani, A. Diedhiou, and T. Lebel. 2005. Rainfall estimation in the Sahel. Part II: evaluation of rain gauge networks in the CILSS countries and objective intercomparison of rainfall products. Journal of Applied Meteorology 44: 1707–1722.

Allen, R. G., L. S. Pereira, D. Raes, and M. Smith. 1998. Crop evapotranspiration. Guidelines for computing crop water requirements. FAO Irrigation and drainage paper 56. Volume 300:D05109. FAO, Rome, Italy.

Allen, R. G., M. Tasumi, A. Morse, and R. Trezza. 2005. A Landsat-based energy balance and evapotranspiration model in Western US water rights regulation and planning. Irrigation and Drainage Systems 19:251–268.

Almazroui, M. 2011. Calibration of TRMM rainfall climatology over Saudi Arabia during 1998–2009. Atmospheric Research 99:400–414.

Anderson, M. C., J. M. Norman, J. R. Mecikalski, J. A. Otkin, and W. P. Kustas. 2007. A climatological study of evapotranspiration and moisture stress across the continental United States based on thermal remote sensing: 1. Model formulation. Journal of Geophysical Research—Atmospheres 112: D10.

Anderson, M. C., C. Hain, B. Wardlow, A. Pimstein, J. R. Mecikalski, and W. P. Kustas. 2011. Evaluation of drought indices based on thermal remote sensing of evapotranspiration over the continental United States. Journal of Climate 24:2025–2044.

Beck, C., J. Grieser, B. Rudolf, and U. Schneider. 2005. A new monthly precipitation climatology for the global land areas for the period 1951 to 2000. Geophysical Research Abstracts 7:07154.

Brutsaert, W., and H. Stricker. 1979. An advection-aridity approach to estimate actual regional evapotranspiration. Water Resources Research 15:443–450.

Chen, J., J. Li, Z. Zhang, and S. Ni. 2014. Long-term groundwater variations in Northwest India from satellite gravity measurements. Global and Planetary Change 116:130–138.

Chokngamwong, R., and L. S. Chiu. 2008. Thailand daily rainfall and comparison with TRMM products. Journal of Hydrometeorology 9:256–266.

Cleveland, R. B., W. S. Cleveland, and I. Terpenning. 1990. STL: a seasonal-trend decomposition procedure based on loess. Journal of Official Statistics 6:3.

De Bruin, H. A. R., and J. N. M. Stricker. 2000. Evaporation of grass under nonrestricted soil moisture conditions. Hydrological Sciences Journal 45:391–406.

DeJong, R., J. Verbesselt, M. Schaepman, and S. DeBruin. 2012. Trend changes in global greening and browning: contribution of short-term trends to longer-term change. Global Change Biology 18:642–655.

Dinku, T., P. Ceccato, E. Grover-Kopec, M. Lemma, S. J. Connor, and C. F. Ropelewski. 2007. Validation of satellite rainfall products over East Africa's complex topography. International Journal of Remote Sensing 28:1503–1526.

Duan, Z., and W. G. M. Bastiaanssen. 2013. First results from Version 7 TRMM 3B43 precipitation product in combination with a new downscaling–calibration procedure. Remote Sensing of Environment 131:1–13.

Ershadi, A., M. F. McCabe, J. P. Evans, N. W. Chaney, and E. F. Wood. 2014. Multi-site evaluation of terrestrial evaporation models using FLUXNET data. Agricultural and Forest Meteorology 187:46–61.

Famiglietti, J. S., M. Lo, S. L. Ho, J. Bethune, K. J. Anderson, T. H. Syed, S. C. Swenson, C. R. de Linage, and M. Rodell. 2011. Satellites measure recent rates of groundwater depletion in California's Central Valley. Geophysical Research Letters 38:000–000.

Fisher, J. B., K. P. Tu, and D. D. Baldocchi. 2008. Global estimates of the land–atmosphere water flux based on monthly AVHRR and ISLSCP-II data, validated at 16 FLUXNET sites. Remote Sensing of Environment 112:901–919.

Fisher, J. B., et al. 2009. The land-atmosphere water flux in the tropics. Global Change Biology 15:2694–2714.

Fisher, J. B., R. J. Whittaker, and Y. Malhi. 2011. ET come home: potential evapotranspiration in geographical ecology. Global Ecology and Biogeography 20:1–18.

Heidinger, H., C. Yarlequé, A. Posadas, and R. Quiroz. 2012. TRMM rainfall correction over the Andean Plateau using wavelet multi-resolution analysis. International Journal of Remote Sensing 33:4583–4602.

Hofhansl, F., J. Kobler, J. Ofner, S. Drage, E.-M. Pölz, and W. Wanek. 2014. Sensitivity of tropical forest aboveground productivity to climate anomalies in SW Costa Rica. Global Biogeochemical Cycles 28:1437–1454.

Houborg, R., J. B. Fisher, and A. K. Skidmore. 2015. Advances in remote sensing of vegetation function and traits. International Journal of Applied Earth Observation and Geoinformation 43:1–6.

Iqbal, N., F. Hossain, H. Lee, and G. Akhter. 2016. Satellite gravimetric estimation of groundwater storage variations over Indus Basin in Pakistan. IEEE Journal of Selected Topics in Applied Earth Observations and Remote Sensing 9:3524–3534.

Jiménez-Román, J. A., E. González-Jiménez, and J. Mateo-Vega, editor. 2001. Perspectives for the integrated management of the Tempisque River Basin, Costa Rica. Organization for Tropical Studies, San Jose, Costa Rica.

Karger, D. N., O. Conrad, J. Böhner, T. Kawohl, H. Kreft, R. W. Soria-Auza, N. E. Zimmermann, H. P. Linder, and M. Kessler. 2017. Climatologies at high resolution for the earth's land surface areas. Scientific Data 4:170122.

Karnieli, A., N. Agam, R. Pinker, M. Anderson, M. Imhoff, G. Gutman, and N. Panov. 2010. Use of NDVI and land surface temperature for drought assessment: merits and limitations. Journal of Climate 23:618–633.

Kustas, W. P., J. M. Norman, C. R. Hain, J. R. Mecikalski, L. Schultz, M. P. González-Dugo, C. Cammalleri, G. d'Urso, A. Pimstein, and F. Gao. 2011. Mapping daily evapotranspiration at field to continental scales using geostationary and polar orbiting satellite imagery. Hydrology and Earth System Sciences 15:223.

Kuzdas, C., B. P. Warner, A. Wiek, R. Vignola, M. Yglesias, and D. L. Childers. 2016. Sustainability assessment of water governance alternatives: the case of Guanacaste Costa Rica. Sustainability Science 11:231–247.

Lin, B. B. 2007. Agroforestry management as an adaptive strategy against potential microclimate extremes in coffee agriculture. Agricultural and Forest Meteorology 144:85–94.

Lin, B. B. 2010. The role of agroforestry in reducing water loss through soil evaporation and crop transpiration in coffee agroecosystems. Agricultural and Forest Meteorology 150: 510–518.

Maes, W. H., P. Gentine, N. E. C. Verhoest, and D. G. Miralles. 2018. Potential evaporation at eddy-covariance sites across the globe. Hydrology and Earth System Sciences 2018:1–33. https://doi.org/10.5194/hess-2017-682.

Magaña, V., J. A. Amador, and S. Medina. 1999. The midsummer drought over Mexico and Central America. Journal of Climate 12:1577–1588.

Maldonado, T., A. Rutgersson, E. Alfaro, J. Amador, and B. Claremar. 2016. Interannual variability of the midsummer drought in Central America and the connection with sea surface temperatures. Advances in Geosciences 42:35–50.

Mangan, J. M., J. T. Overpeck, R. S. Webb, C. Wessman, and A. F. Goetz. 2004. Response of Nebraska Sand Hills natural vegetation to drought, fire, grazing, and plant functional type shifts as simulated by the century model. Climatic Change 63:49–90.

McCabe, M. F., A. Ershadi, C. Jimenez, D. G. Miralles, D. Michel, and E. F. Wood. 2016. The GEWEX LandFlux project: evaluation of model evaporation using tower-based and globally gridded forcing data. Geoscientific Model Development 9:283–305.

McKee, T. B., N. J. Doesken, and J. Kleist. 1993. The relationship of drought frequency and duration to time scales. Pages179–183 *in* Proceedings of the 8th Conference on Applied Climatology. Volume 19. American Meteorological Society, Boston, Massachusetts, USA.

Melton, F. S., et al. 2012. Satellite irrigation management support with the terrestrial observation and prediction system: a framework for integration of satellite and surface observations to support improvements in agricultural water resource management. IEEE Journal of Selected Topics in Applied Earth Observations and Remote Sensing 5:1709–1721.

Monteith, J. L. 1965. Evaporation and environment. Symposia of the Society for Experimental Biology 19:4.

Muhs, D. R. 1998. Activation of Great Plains dune sand during the 1930s drought. Geological Society of America 1998 Annual Meeting Abstracts with Programs. Geological Society of America, Boulder, Colorado, USA.

Nicholson, S. E., et al. 2003. Validation of TRMM and other rainfall estimates with a high-density gauge dataset for West Africa. Part II: validation of TRMM rainfall products. Journal of Applied Meteorology 42:1355–1368.

Otkin, J. A., M. C. Anderson, C. Hain, I. E. Mladenova, J. B. Basara, and M. Svoboda. 2013. Examining rapid onset drought development using the thermal infrared-based evaporative stress index. Journal of Hydrometeorology 14:1057–1074.

Patel, N. R., P. Chopra, and V. K. Dadhwal. 2007. Analyzing spatial patterns of meteorological drought using standardized precipitation index. Meteorological Applications 14:329–336.

Penuelas, J., C. Gordon, L. Llorens, T. Nielsen, A. Tietema, C. Beier, P. Bruna, B. Emmett, M. Estiarte, and A. Gorissen. 2004. Nonintrusive field experiments show different plant responses to warming and drought among sites, seasons, and species in a north–south European gradient. Ecosystems 7:598–612.

Peters, A. J., E. A. Walter-Shea, L. Ji, A. Vina, M. Hayes, and M. D. Svoboda. 2002. Drought monitoring with NDVI-based standardized vegetation index. Photogrammetric Engineering and Remote Sensing 68:71–75.

Pettorelli, N., J. O. Vik, A. Mysterud, J. M. Gaillard, C. J. Tucker, and N. C. Stenseth. 2005. Using the satellite-derived NDVI to assess ecological responses to environmental change. Trends in Ecology and Evolution 20:503–510.

Priestley, C. H. B., and R. J. Taylor. 1972. On the assessment of surface heat flux and evaporation using large-scale parameters. Monthly Weather Review 100:81–92.

Quesada, C. A., and J. Lloyd. 2016. Soil-vegetation interactions in Amazonia. Pages 267–299 *in* L. Nagy, B. Forsberg, and P. Artaxo, editor. Interactions between biosphere, atmosphere and human land use in the Amazon Basin. Springer, Berlin, Germany.

Rammig, A., et al. 2018. A generic pixel-to-point comparison for simulated large-scale ecosystem properties and ground-based observations: an example from the Amazon region. Geoscientific Model Development Discussions. https://doi.org/10.5194/gmd-2018-182

Reid, K., and L. R. Oki. 2014. Evaluation of ornamental plant performance on four deficit irrigation levels: working with industry to promote sustainable plant choices for summer-dry regions. Acta Horticulturae 1112:155–162.

Ryu, Y., et al. 2011. Integration of MODIS land and atmosphere products with a coupled-process model to estimate gross primary productivity and evapotranspiration from 1 km to global scales. Global Biogeochemical Cycles 25: GB4017.

Saleska, S. R., K. Didan, A. R. Huete, and H. R. Da Rocha. 2007. Amazon forests green-up during 2005 drought. Science 318:612–612.

Senay, G. B., M. Budde, J. P. Verdin, and A. M. Melesse. 2007. A coupled remote sensing and simplified surface energy balance approach to estimate actual evapotranspiration from irrigated fields. Sensors 7:979–1000.

Shah, N. H., and G. M. Paulsen. 2003. Interaction of drought and high temperature on photosynthesis and grain-filling of wheat. Plant and Soil 257:219–226.

Sistema Nacional de Áreas de Conservación (SINAC). 2015. Cartografía base para el Inventario Forestal Nacional de Costa Rica 20132014. Programa REDD-CCAD-GIZ, San José, Costa Rica. http://www.sirefor.go.cr/?wpfb_dl=7

Sönmez, F. K., A. U. Kömüscü, A. Erkan, and E. Turgu. 2005. An analysis of spatial and temporal dimension of drought vulnerability in Turkey using the standardized precipitation index. Natural Hazards 35:243–264.

Tsakiris, G., D. Pangalou, and H. Vangelis. 2007. Regional drought assessment based on the Reconnaissance Drought Index (RDI). Water Resources Management 21: 821–833.

Tscharntke, T., et al. 2011. Multifunctional shade-tree management in tropical agroforestry landscapes–a review. Journal of Applied Ecology 48:619–629.

Tuberosa, R., and S. Salvi. 2006. Genomics-based approaches to improve drought tolerance of crops. Trends in Plant Science 11:405–412.

Tukey, J. W. 1949. Comparing individual means in the analysis of variance. Biometrics 1:99–114.

United Nations Office for the Coordination of Humanitarian Affairs (UNOCHA). 2014. Drought in Central America (Situation No. 1). Central America: Regional Office for Latin America and the Caribbean in collaboration with humanitarian partners from Guatemala, Honduras, and El Salvador. https://reliefweb.int/sites/reliefweb.int/files/resources/Drought%20in%20Central%20America.pdf

United Nations Office for the Coordination of Humanitarian Affairs (UNOCHA). 2016. Central America Sub-Regional Analysis: El Salvador, Guatemala and Honduras (Humanitarian Needs Overview No. 1). https://www.humanitaria nresponse.info/sites/www.humanitarianresponse.info/files/documents/files/2016-hno-centralamerica-7jan.pdf

Vicente-Serrano, S. M., et al. 2013. Response of vegetation to drought time-scales across global land biomes. Proceedings of the National Academy of Sciences USA 110:52–57.

Yong, B., L. L. Ren, Y. Hong, J. H. Wang, J. J. Gourley, S. H. Jiang, X. Chen, and W. Wang. 2010. Hydrologic evaluation of Multisatellite Precipitation Analysis standard precipitation products in basins beyond its inclined latitude band: a case study in Laohahe basin, China. Water Resources Research 46(7).

Zuur, A. F., R. J. Fryer, I. T. Jolliffe, R. Dekker, and J. J. Beukema. 2003. Estimating common trends in multivariate time series using dynamic factor analysis. Environmetrics 14:665–685.

Supporting Information

Additional supporting information may be found online at: http://onlinelibrary.wiley.com/doi/10.1002/eap.1834/full

Data Availability

Data are available from Figshare: https://doi.org/10.6084/m9.figshare.7253414; https://doi.org/10.6084/m9.figshare.7253705; https://doi.org/10.6084/m9.figshare.7255862; https://doi.org/10.6084/m9.figshare.7271384; https://doi.org/10.6084/m9.figshare.7271408; https://doi.org/10.6084/m9.figshare.7271426; https://doi.org/10.6084/m9.figshare.7271432; https://doi.org/10.6084/m9.figshare.7271435; https://doi.org/10.6084/m9.figshare.7271438; https://doi.org/10.6084/m9.figshare.7271441; https://doi.org/10.6084/m9.figshare.7271495; https://doi.org/10.6084/m9.figshare.7271504; https://doi.org/10.6084/m9.figshare.7271507; https://doi.org/10.6084/m9.figshare.7271528; https://doi.org/10.6084/m9.figshare.7271555; https://doi.org/10.6084/m9.figshare.7272716.